Title

Reactive iron, not fungal community, drives organic carbon oxidation potential in floodplain soils

Authors

Naughton, Hannah R

Tolar, Bradley B

Dewey, Christian

et al.

Publication Date

2023-03-01

DOI

10.1016/j.soilbio.2023.108962

Soil Biology and Biochemistry 178 (2023) 108962

Contents lists available at ScienceDirect

Soil Biology and Biochemistry

journal homepage: www.elsevier.com/locate/soilbio

Reactive iron, not fungal community, drives organic carbon oxidation potential in floodplain soils

Hannah R. Naughton [a,*,1], Bradley B. Tolar [a,2], Christian Dewey [a], Marco Keiluweit [b,3], Peter S. Nico [c,d], Scott Fendorf [a]

[a] Earth System Science Department, Stanford University, Stanford, CA, USA
[b] Stockbridge School of Agriculture, University of Massachusetts, Amherst, MA, USA
[c] Lawrence Berkeley National Laboratory, Earth and Environmental Sciences Area, Berkeley, CA, USA
[d] Department of Environmental Science, Policy and Management, UC Berkeley, Berkeley, CA, USA

ARTICLE INFO

Keywords:
Oxidative degradation
Soil organic carbon
Enzyme activity
Redox-active metals

ABSTRACT

Wetlands host ~20% of terrestrial organic carbon and serve as a major sink for atmospheric carbon. Anoxic soils and sediments accrue soil organic carbon (SOC) partly by hampering the activity of extracellular oxidative enzymes that break down phenolic polymers. Upon aeration, fungal-driven oxidative enzymatic depolymerization and microbial respiration of released monomers ensue. Redox-active metals can simultaneously catalyze abiotic nonspecific oxidation of SOC, notable examples including Mn(III) or Fe(II) through Fenton-like, hydrogen peroxide-catalyzed oxidative radical production. However, the extent of reactive metal contributions to biotic and abiotic SOC degradation is not understood in the context of natural environments with diverse redox chemistry. We tested the relative contributions of fungi, Mn(III) and Fe(II) to phenolic substrate (L-DOPA) oxidation in floodplain soils representing a range of transient redox conditions driven by permanent vs. periodic flooding. Phenol oxidative potential was highest in permanently flooded soils with fewer fungal taxa known for observed (per)oxidase activity and instead correlated with HCl-extractable Fe(II), Fe(total) and Fe(II)/Fe(total), suggesting a specific role of Fe(II). Fe(II) additions enhanced phenol oxidative potential in sterilized and non-sterilized soils in the presence of hydrogen peroxide, indicating abiotic Fe-mediated radical chemistry could significantly enhance wetland SOC oxidative depolymerization throughout redox-active floodplain soils. Fungal community composition did not correlate to phenol oxidative potential overall and only more oxic soils adjacent to the river with diverse fungal communities showed declining oxidative potential after sterilization. Mn(III) addition did not significantly enhance phenol oxidative potential across all soils, although it appeared to drive fungal-mediated oxidative potential in the most aerated floodplain soils. Understanding how metals mediate SOC depolymerization as abiotic oxidants or microbially-harnessed enzyme cofactors and substrates in soils under variable hydrologic controls will improve our ability to represent depolymerization in terrestrial carbon models in wetland and other frequently saturated soils.

1. Introduction

Of the world's approximate 2800 Pg terrestrial carbon, an estimated 513 ± 256 Pg resides in wetlands – accounting for 9–27% of total terrestrial carbon, depending on the soil depth considered (Bridgham et al., 2006; Lal, 2008; Mitsch et al., 2013; Jackson et al., 2017). Saturated soils preserve soil organic carbon (SOC) by limiting oxygen diffusion into the soil, which inhibits microbial extracellular oxidative enzymes that depend on oxygen to degrade polyphenolic and other complex macromolecules that cannot be hydrolyzed (Wong, 2009; Bugg et al., 2011).

Ascomycota and Basidiomycota fungi dominate plant litter

Abbreviations: SOC, Soil organic carbon.

* Corresponding author.
E-mail address: hnaughton@umass.edu (H.R. Naughton).
[1] Present Address: Lawrence Berkeley National Laboratory, Earth and Environmental Sciences Area, Berkeley, CA.
[2] Present Address: Department of Biology & Marine Biology, University of North Carolina Wilmington, Wilmington, NC.
[3] Present Address: Institute of Earth Surface Dynamics, University of Lausanne, Lausanne, Switzerland.

https://doi.org/10.1016/j.soilbio.2023.108962
Received 29 May 2022; Received in revised form 13 January 2023; Accepted 17 January 2023
Available online 19 January 2023

decomposition in the traditional paradigm through the production of hydrolytic and oxidative extracellular enzymes that catalyze the depolymerization of biopolymers (Fontaine and Barot, 2005; Sinsabaugh, 2010). Only strong oxidants, such as those produced by fungal phenol oxidase and peroxidase extracellular enzymes, can cleave chemically complex lignin structures and expose cellulose and hemicellulose for degradation by a broader assemblage of microorganisms (Wong 2009). Free-living saprotrophic fungi mediate carbohydrase and phosphatase mining of less complex organic matter, whereas ectomycorrhizal fungi specialize in the degradation of more complex and N-containing organic compounds using protease and peroxidase enzymes (Talbot et al., 2013, 2015). In this way, fungal enzymes are thought to control the rate of depolymerization of organic carbon and production of oligomers and monomers that can be taken up for respiration or preserved through mineral protection (Moorhead and Sinsabaugh, 2000; Schimel and Weintraub, 2003; Vidal et al., 2021). Notably, the oxidase and peroxidase enzymes require oxygen or oxygen-generated hydrogen peroxide (H_2O_2) to function, implying limited enzymatic depolymerization potential in reducing floodplain soils.

A number of studies have directly related the inhibition of oxidative enzymes such as polyphenol oxidases and peroxidases and accumulation of phenolic compounds to anoxic conditions (Freeman et al., 2001, 2004; Zibilske and Bradford, 2007; Fenner and Freeman, 2011). However, lab studies and field observations also connect reduced iron (Fe(II)) to oxidation of dissolved organic matter and phenols in particular (Van Bodegom et al., 2005; Page et al., 2013; Wang et al., 2017; Xie et al., 2020). This "iron gate" process implies that phenolic oxidative degradation occurs under oxygen-limited conditions and may be heavily mediated by actors other than extracellular oxidative enzymes.

Metal-facilitated SOC oxidation occurs abiotically through the production of reactive oxygen species (ROS), but microorganisms also harness metals to depolymerize organic matter. In the classic example of manganese, microorganisms oxidize Mn(II) with manganese peroxidase (MnP) to the potent oxidant Mn(III). When stabilized by ligands such as oxalic acid, pyrophosphate or phenolics (Keiluweit et al., 2015; Oldham et al., 2015, 2017), Mn(III) directly oxidizes phenolic and nonphenolic compounds and depolymerizes lignocellulose (Perez and Jeffries, 1992; Hofrichter, 2002). Other extracellular enzymes, including laccases, versatile peroxidases, and lignin peroxidase through an indirect mechanism, also oxidize Mn(II) to Mn(III) (Popp et al., 1990; Muñoz et al., 1997; Gómez-Toribio et al., 2001; Hofrichter, 2002). Mn therefore contributes to phenol oxidation biotically through its role as a substrate of oxidative enzymes, particularly in the presence of H_2O_2, and abiotically as the ligand-stabilized oxidation product Mn(III) (Hofrichter 2002).

While not a direct substrate of extracellular oxidative enzymes like Mn(II), Fe(II) is harnessed by microorganisms to produce oxidizing radicals for non-specific degradation of plant litter (Shah et al., 2015; Jones et al., 2020). Microorganisms benefit from ROS-mediated depolymerization by triggering reactions similar to the abiotic, dark reactions that produce ROS from Fe(II) (Luther, 2010; Page et al., 2013; Minella et al., 2015; Tong et al., 2016). The classic example is Fenton-style reactions, which produce ROS, most notably the hydroxyl radical •OH, via the reaction of Fe(II) with H_2O_2 (Moffett and Zika, 1987; Millero and Sotolongo, 1989; King et al., 1995; Pignatello et al., 2006). Hydrogen peroxide is formed abiotically via oxygen reduction by Fe(II) or biotically through microbial reduction of oxygen (Aguirre et al., 2005; Kim et al., 2007; Keenan and Sedlak, 2008; Diaz et al., 2013; Sheng et al., 2014; Han et al., 2019). Hydroxyl radicals can diffuse into complex organic structures such as lignin, a key ability not thought possible by extracellular enzymes (Srebotnik et al., 1988; Flournoy et al., 1991; Blanchette et al., 1997). Hydroxyl radical is capable of oxidizing the most stable molecular bonds and can depolymerize lignin (Eastwood et al., 2011). Reduced iron species therefore may strongly contribute to polyphenolic degradation at oxic-anoxic interfaces through Fenton chemistry and H_2O_2 generation (Hall and Silver, 2013).

Metal-induced ROS production and ensuing oxidative degradation of organic matter requires either temporal or spatial variation in oxygen levels. Within oxygen-limited zones, where biological demand exceeds supply, dissimilatory Mn and Fe reduction produce Mn(II) and Fe(II) (Moffett and Zika, 1987; Page et al., 2013; Xiang et al., 2013; Tong et al., 2016). However, oxic conditions are required to produce the H_2O_2 that triggers Fe(II) or peroxidase oxidation. It is not likely coincidence that abiotic Fe(II)-mediated organic carbon oxidation has been observed in environments experiencing frequent water saturation –*e.g.* rain forests, floodplains, and bogs and fens – with active Fe(II)/Fe(III) redox cycling (Inubushi et al., 1984; Liptzin and Silver, 2009; Dubinsky et al., 2010; Lipson et al., 2010) and often significant H_2O_2 production (Hall and Silver, 2013; Yuan et al., 2022). Floodplains encompass a range of redox conditions over space and time from relatively oxic in meander surface soils to periodically reducing in subsurface soils, and completely reducing in river and cutoff channels. Moreover, changing snowpack and monsoon dynamics in a warming world will affect hydrology and biogeochemical functioning of floodplain systems globally (Martinez-Villalobos and Neelin, 2018; Mote et al., 2018). We therefore selected the well-studied subalpine floodplain site of the East River at Crested Butte, CO, to investigate the potential for Fe and possibly Mn abiotic oxidation of SOC over a range of hydrologic and thus redox conditions in otherwise similarly formed soils.

Here, we assessed the extent to which abiotic versus microbial processes drive extracellular oxidative potential, the rate-limiting step of litter decomposition. We used two complementary methods: laboratory incubations coupled with phenol oxidative potential assays and correlations of field soil geochemical and fungal components with phenol oxidative potential. We performed oxidative enzyme assays using L-3,4-dihydroxyphenylalanine (L-DOPA) as a monomeric lignin representative with a characteristic absorption band upon oxidation. L-DOPA is an unselective substrate for a variety of oxidative enzymes and can also be oxidized directly by Mn(III) and Fenton-produced •OH (Sinsabaugh, 2010), making it ideal for comparing various biotic and abiotic phenolic oxidation pathways. Assays were performed with unamended soil and added Mn(III) and Fe(II) to test for Mn(III) contributions to organic carbon oxidation as reported in forest soils (Jones et al., 2020) and Fenton-mediated oxidation via Fe(II) as reported in aquatic or frequently saturated environments (Hall and Silver, 2013; Page et al., 2013; Wang et al., 2017). An autoclave sterilization treatment was used to control for microbial oxidative enzyme activity, thus isolating abiotic, metal-catalyzed oxidation processes. Fungal decomposers and Mn were expected to increase phenol oxidative potential in more oxic soils, whereas Fe-catalyzed phenol oxidation was expected to dominate in more reducing soils. Permanent saturation was expected to limit all phenol oxidative processes and enhance SOC storage. We discovered diverse mechanisms of oxidative depolymerization and decomposition of organic matter operating over short spatial distances that, given that wetland soils contain roughly 20% of global soil organic matter, are likely to affect calculations of regional C sinks and fluxes.

2. Methods

2.1. Sample collection and processing

2.1.1. Field site and soil sampling

Soils were collected in September of 2020 from the East River floodplain near Crested Butte, Colorado, USA. These floodplain soils are part of the Gas Creek series, a Sandy-Skeletal, mixed, frigid Typic Haplaquolls. We sampled two hydrologically distinct sites at our focus meander "Z" off the Brush Creek trail at approximately 38° 88′ 98.58″ N by 106° 90' 83.85″ W: two meander soil profiles from surface to unconsolidated material that are seasonally flooded, and an adjacent cutoff oxbow channel that is permanently saturated (Fig. 1). The meander is dominated by bog birch (*Betula pumila* L.) and willow (*Salix monticola* L.) species with scattered cinquefoil (*Potentilla gracilis* Douglas ex Hook.)

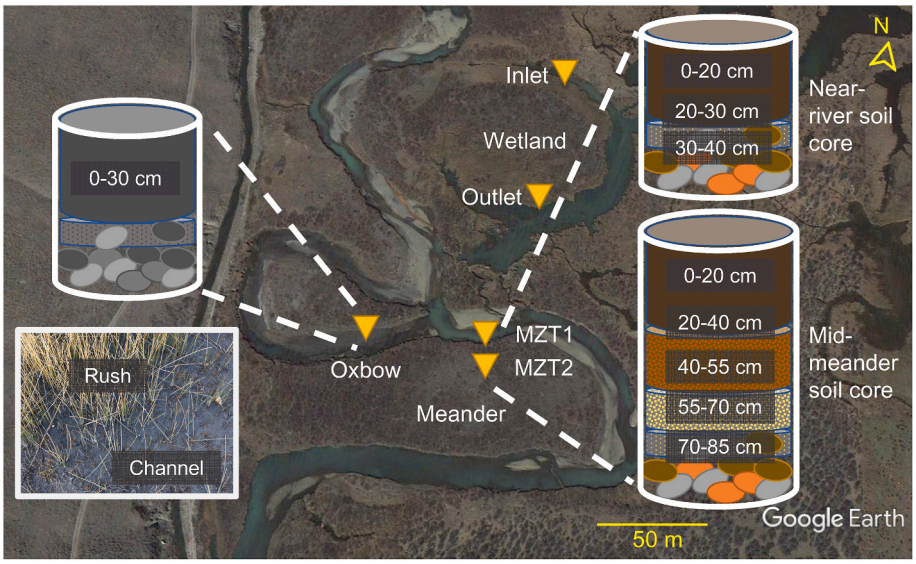

Fig. 1. East River field site off the Brush Creek trail showing Meander Z and associated oxbow and wetland. Soil samples are indicated by core, depth and plant labels. Cores are not drawn precisely to scale or true color.

and grasses, whereas the oxbow is dominated by spike-rush and sedge (*Eleocharis palustris* (L.) Roem. & Schult. and *Carex utriculata* Boott). Seasonal flooding occurs between April and June due to snowmelt. Over the summer, the floodplain water table recedes into the subsurface. Late season soils therefore experience redox gradients with depth and lateral distance to the oxic river.

Along a transect of five well and permeameter sampling sites (Meander Z Transect, MZT), we took soil cores near the two northern-most well clusters. MZT1 was within 2 m of the river and the least developed soil along the transect (roughly 40 cm deep, "MZT1 0–20 cm", "MZT1 20–30 cm" and "MZT1 30–40 cm"), whereas MZT2 was inland and represented the most developed portion of this transect (~80 cm core was accessible as the gravelly bottom continued to cave in during sampling) and split into five depths: "MZT2 0–20 cm", *ibid.* 20–40, 40–55, 55–70 and 70–85 cm. The oxbow channel was saturated but had no standing water. We sampled both the unvegetated ("oxbow channel") and proximal (1 m separation) spike rush-vegetated portions of the channel ("oxbow rush"). Because of their permanently saturated status, the oxbow sites were only sampled down to 30 cm. We were interested in the oxbow as a fully reduced site where differences in plant cover rather than depth, which was the primary interest in the meander cores, were likely to influence redox conditions. Soils were also obtained in September of 2017 for the same sites plus from a saturated, older cutoff oxbow across the river called "wetland" due to its position within a larger wetland complex (Fig. 1). Geochemical and oxidative activity assays for these soils were compared to the 2020 dataset in the Supplementary Material to confirm similar findings over time.

A 5 cm diameter x 15 cm stainless steel corer with PVC sleeves fitted with a slide hammer (AMS) was used to collect samples in the field. Cores were contained within PVC core sleeves with PE caps that were then placed into gallon Ziploc bags for transport out of the field. Within hours of sampling, bags with soil cores were placed into mylar bags with oxygen scrubbers (USA Emergency Supply) and heat-sealed to preserve anaerobic conditions. The bags were refrigerated at 4 °C for two days until shipment over ice to Stanford University. Once in the lab, cores were taken into an anaerobic glovebag with 97.5%:2.5% N_2:H_2 attached to a Coy transfer chamber. Cores were removed from their sleeves and the top and bottom centimeters sliced off to minimize influence of environmental conditions during collection and transport. Cores were then sieved through 2 mm mesh at field moisture conditions to remove coarse material. Half of processed cores were stored in Ball mason jars at 4 °C for downstream experiments, including enzyme assays. Quick processing of soils and minimization of anaerobic headspace in mason jars limited hydrogen exposure of samples and related stimulation of Fe-reducing bacteria. Fifteen-mL Falcon tubes were filled with sieved core and frozen at −80 °C for molecular biology work, and the remainder of soil was freeze-dried (Labconco FreeZone 4.5L Benchtop Freeze Dry System) for 48 h for geochemical analysis. Freeze-dried samples were stored in mason jars in the glovebag to preserve reduced redox-active species.

2.1.2. Nutrient content

Soil C and N content were measured on a Carlo Erba NA1500 Elemental Analyzer. Briefly, 18–22 mg of soil and five atropine standards (0.4–4 mg) were weighed into tin capsules and measured by the elemental analyzer. To remove carbonate, separate samples were weighed into pressed silver capsules (Elemental Microanalysis) that received 50 μL of 1% HCl. These samples were fumigated with concentrated HCl for 68 h (Walthert et al., 2010) and then dried in the fumigation chamber with silica beads for 48 h and oven-dried for 24 h at 60 °C. Samples were placed into new silver foils for elemental analysis of organic C.

2.1.3. Metal content and iron speciation

Elemental composition of soils was measured by X-ray fluorescence spectrometry (SPECTRO XEPOS HE XRF Spectrometer). Freeze-dried, agate-ground samples were further ground with a Wig-L-Bug® grinding mill in small plastic capsules with silica beads, suspended with isopropyl alcohol, and placed by transfer pipet on the sample holder in a thin film. Mineralogy was qualitatively assessed by X-ray diffraction (XRD, Rigaku MiniFlex 600 Benchtop X-ray Diffraction System). Subsamples of freeze-dried, agate-ground soils stored anaerobically in the glove bag were also prepared for extended X-ray absorption fine structure (EXAFS) spectroscopic analysis at the Fe K-edge at the Stanford Synchrotron Radiation Lightsource (SSRL in Menlo Park, CA, USA) on beamline 7-3. Soil mineralogy was only determined on the 2017 samples and considered representative of the 2020 samples (see Supplementary Materials).

Acid extracts were performed to measure reactive Mn and Fe. Solutions of 0.5 M and 1.0 M HCl were prepared in acid-washed glassware and N_2-purged for 1 h with a bubbler inserted into a 1 L, acid-washed borosilicate bottle of acid on a stir plate. Triplicate 0.25 g of freeze-dried soil in 75 mL acid-washed glass serum vials received 20 mL of 0.5 M HCl and were sealed with 20 mm acid-washed butyl septa

(Chemglass Life Sciences). Samples were shaken for 2 h at 145 rpm on an orbital shaker (VWR). Subsamples of slurry, 1.5 mL each, were added to 2 mL microcentrifuge tubes (Thomas Scientific) in an anaerobic glovebag and centrifuged for 3 min at 13,000×*g*. Supernatant (0.5 mL) was added to 1.5 mL microcentrifuge tubes, received 0.5 mL anoxic 1 M HCl, and was analyzed by the ferrozine assay (Naughton et al., 2021). Supernatant (0.5 mL) was also added to 9.5 mL of 3% HNO_3 in a 15 mL Falcon tube for Fe, Mn and S analysis by ICP-OES (Thermo Scientific ICAP 6300 Duo View).

2.2. DNA sequencing and analysis

A MoBio PowerSoil® DNA Isolation Kit was used to extract DNA from 0.5 g of field-moist soils in duplicate. Manufacturer instructions were followed except that soils in PowerBead tubes were incubated at 65 °C for 10 min before further processing to enhance DNA extraction from these soils, and only 50 μL of Solution C6 was used to elute DNA for a more concentrated solution. DNA quality was confirmed by ethidium bromide-dyed agarose gel electrophoresis and Nanodrop spectrophotometry (Thermo Fisher), and quantity was determined by Qubit® 2.0 using the Qubit™ dsDNA HS Assay Kit (Invitrogen).

Amplification and iTag sequencing were performed on an Illumina MiSeq running 2 × 300 bp at the DOE Joint Genome Institute (JGI; Walnut Creek, CA, USA). Fungal ITS libraries were created by amplification using ITS2 primers ITS9 (5′-GAACGCAGCRAAIIGYGA3'-, Ihrmark et al. (2012)) and ITS4 (5′-TCCTCCGCTTATTGATATGC-3', Gardes and Bruns (1993)) following the JGI iTag protocol. The resulting ITS reads were analyzed in mothur (Schloss et al., 2009) using the CRG Bioinformatics Core Protocol for ITS amplicons (https://github.com/biocorecrg/microbiome_procedures/blob/master/README_mothur_ITS.txt). Briefly, chimeras were first removed before classification of ITS reads according to the UNITE Database (mothur full version February 04, 2020; https://unite.ut.ee/repository.php, Nilsson et al. (2019)), then OTUs were constructed at 95% sequence similarity using the ACG method in mothur. The constructed ITS OTUs were further analyzed in R Studio using the phyloseq package (McMurdie and Holmes, 2013).

Fungal guilds, including saprotrophs, symbionts (endo- and ectomycorrhizae, the latter abbreviated "ECM"), Basidiomycota + Ascomycota ("BA"), and white rot fungi were assigned using FUNGuild (Nguyen et al., 2016). Of 24,284 fungal taxa observed, 3048 were assigned a fungal guild. Alpha diversity measures were calculated prior to pruning of singletons, after which relative abundance of guilds and taxonomic groups was calculated. Saprotrophs were identified from the "Trophic Mode" designations, ectomycorrhizal fungi from the "Guild" designation, and rot type from the "Trait" designation. We double-counted taxa listed with more than one trait, guild or trophic mode and counted taxa with additional designations such as pathotroph for the purposes of sub-setting the sequence data into functional guilds. Chao1 richness and Shannon diversity were calculated for each fungal group to be used in correlations with SOC and phenol oxidative potential. We chose to test oxidative potential as relates to Basidiomycota + Ascomycota, saprotrophs, and ectomycorrhizal fungi for their known contribution to lignin degradation and versus all fungi to test their ability to proxy decomposer guilds.

2.3. Enzyme assays

2.3.1. Traditional L-DOPA activity assays

Spectrophotometric assays were performed to assess the phenol oxidation capacity of soils using l-3,4-dihydroxyphenylalanine (L-DOPA) as a phenolic substrate. These assays are traditionally used to quantify the oxidative activity of phenol oxidase and peroxidase, hence the term "enzyme assays" (Saiya-Cork et al., 2002; Allison and Vitousek, 2004; DeForest, 2009). Because the assay also responds to oxidation by Mn(III), •OH, and organic radicals not directly produced by oxidative enzyme activity (Sinsabaugh 2010), we will refer to these experiments as "L-DOPA assays" measuring "(phenol) oxidative potential".

L-DOPA was chosen as substrate due to its prevalence in soil decomposition literature, low specificity regarding oxidants, and the relatively low sensitivity of its reduction potential to changes in pH (Sinsabaugh, 2010; Bach et al., 2013). A pH 5 buffer, while more acidic than our soils with circumneutral pH (Table 1), is most favorable for phenol oxidase activity and L-DOPA oxidation by peroxidases and is frequently the buffer of choice, making this assay comparable to previous experiments (Saiya-Cork et al. 2002; Allison and Vitousek 2004; DeForest 2009). While Fe(II) and Mn(II) are less soluble under mildly acidic conditions, they are often stabilized by organic ligands such as acetate that mitigate pH effects on solubility, hence our choice of an acetate buffer. For 1 L of solution, 6.804 g of $Na_2(C_2H_3O_2)•3H_2O$ and 1.1 mL glacial acetic acid were added to a 1 L volumetric flask filled to 1 L with milliQ water. L-DOPA (Sigma-Aldrich) substrate solution, 25 mM, was prepared daily by adding warm milliQ water (100 mL microwave-heated) to 493 mg L-DOPA to prevent precipitation. We omitted EDTA in the L-DOPA solution to allow for oxidative enzyme use of metal cofactors and substrates that EDTA would chelate (German et al., 2011) and to allow for the possibility of metal-mediated oxidative activity.

The L-DOPA absorption coefficient was calculated by running the enzyme assay with eight L-DOPA concentrations (0–5 mM in sodium acetate buffer, adding 0–50 μL volumes from 25 mM stock), 50 μL excess mushroom tyrosinase (Sigma-Aldrich) prepared in sterile milliQ water to completely oxidize the L-DOPA, and sodium acetate buffer added to 250 μL. The linear portion of the absorption vs. concentration curve occurred between 0 and 250 μM L-DOPA. A 2 h incubation period was determined ideal as absorbance increased between 0 and 1.5 h but did not significantly change between 1.5 and 2.0 h. Buffer, substrate and enzyme controls were run on the same plate. Each control or L-DOPA concentration level was run in a single column of a clear 96-well plate (Fisher), making 8 experimental replicates.

Soil slurries were prepared by homogenizing 0.5–1.0 g field-moist, refrigerated soil (depending on organic carbon content; less soil was used in C-rich samples to minimize background absorbance) that had been stored for up to two weeks in 125 mL pH 5 sodium acetate buffer using a blender (Hamilton Beach) for 1 min at high speed. In a 96-well plate, each column was used for a single treatment, resulting in 8 replicate wells. For each soil, one column of homogenate control (50 μL buffer and 200 μL soil homogenate) and two assay columns (50 μL substrate plus 200 μL soil homogenate) were used. A buffer control (250 μL buffer) and standard control (200 μL buffer plus 50 μL L-DOPA) were prepared for each 96-well plate in addition to assays for three soil samples. After 2 h of incubation in the dark at room temperature, plates were centrifuged for 3 min at 3000 rpm and 200 μL of supernatant was pipetted into new plates to minimize absorption interference from soil solids. Supernatant absorbances were read on a microplate reader (BioTek Instruments Synergy HTX Multi-Mode Microplate Reader) at 460 nm.

The assay described above specifically targets phenol oxidase activity. Peroxidase activity (e.g. lignin peroxidase, Mn-peroxidase and versatile peroxidase) and Fenton-mediated •OH production require hydrogen peroxide as electron acceptor. To test for these potential drivers of decomposition, we performed the enzyme assay with added 10 μL 0.3% H_2O_2 to every well in the plate at the beginning of the experiment. Three percent H_2O_2 was stored in the dark between uses and diluted 10% with sterile milliQ water for each use.

2.3.2. Oxidative activity attribution to microorganisms vs. metals

An additional series of L-DOPA assays was conducted to assess the relative contribution of extracellular enzymes and reduced metals to organic matter oxidation in lowland soils. Metal addition treatments (Mn(III) and Fe(II)) were chosen to test their role in facilitating phenol oxidation. The concentration of metals added was chosen to match the high end of concentrations found in the soil slurries as determined by

Table 1
Enzyme activities and key characteristics for 2020 soils related to phenol oxidative potential.

Soil	Phenol Oxid. Potential $-H_2O_2$ (μmol g^{-1} h^{-1})[a]	Phenol Oxid. Potential $+H_2O_2$ (μmol g^{-1} h^{-1})[a]	Total C_{org} (%)	Soil C_{org}/N	Fe (total)$_{HCl}$ (mg g^{-1})	$Fe(II)_{HCl}$ (mg g^{-1})	Fe(II)/Fe (total)$_{HCl}$	Mn (total)$_{HCl}$ (mg g^{-1})	Total S (%)	Total Mn (g kg^{-1} soil)	Total Fe (g kg^{-1} soil)	Soil pH
MZT1 0–20 cm	1.6 (0.5)	9.4 (0.6)	2.25 (0.08)	12.6 (0.3)	5.9 (1)	2.86 (0.06)	0.48 (0.08)	0.188 (0.002)	0.0651 (0.0008)	0.297 (0.001)	25.72 (0.03)	7.9 (0.2)
MZT1 20–30 cm	2.1 (0.4)	6.4 (0.6)	1.87 (0.04)	11.0 (0.1)	4.6 (0.2)	1.52 (0.02)	0.33 (0.01)	0.184 (0.005)	0.0522 (0.0007)	0.319 (0.001)	26.99 (0.03)	7.65 (0.02)
MZT1 30–40 cm	1.2 (0.2)	6.6 (0.3)	1.67 (0.02)	10.7 (0.2)	4.3 (0.5)	1.89 (0.04)	0.44 (0.05)	0.196 (0.004)	0.0457 (0.0007)	0.336 (0.001)	27.49 (0.03)	7.65 (0.01)
MZT2 0–20 cm	1.4 (0.3)	8.1 (0.8)	3.6 (0.2)	15.2 (0.6)	5.2 (0.3)	3.84 (0.05)	0.74 (0.05)	0.203 (0.004)	0.0554 (0.0007)	0.287 (0.001)	23.18 (0.03)	7.21 (0.04)
MZT2 20–40 cm	0.9 (0.1)	3 (1)	1.54 (0.07)	11.3 (0.1)	3.81 (0.09)	1.37 (0.05)	0.36 (0.02)	0.168 (0.006)	0.0373 (0.0006)	0.283 (0.001)	26.66 (0.03)	7.56 (0.02)
MZT2 40–55 cm	1.1 (0.5)	1.8 (0.8)	0.86 (0.01)	9.8 (0.1)	2.8 (0.2)	0.35 (0.05)	0.12 (0.02)	0.10 (0.02)	0.0351 (0.0006)	0.294 (0.001)	28.84 (0.03)	7.59 (0.03)
MZT2 55–70 cm	0.5 (0.3)	2.9 (0.3)	0.60 (0.02)	8.5 (0.5)	2.69 (0.06)	0.80 (0.04)	0.3 (0.02)	0.137 (0.008)	0.0287 (0.0006)	0.353 (0.001)	32.90 (0.03)	7.59 (0.02)
MZT2 70–85 cm	0.7 (0.2)	3.0 (0.4)	0.44 (0.02)	7.3 (0.5)	3.4 (0.3)	1.3 (0.2)	0.38 (0.08)	0.167 (0.008)	0.0269 (0.0006)	0.373 (0.001)	30.28 (0.03)	7.49 (0.07)
Oxbow Rush	1.1 (0.1)	7.5 (0.6)	2.28 (0.07)	10.8 (0.2)	5.47 (0.06)	2.86 (0.08)	0.52 (0.02)	0.22 (0.02)	0.0602 (0.0008)	0.363 (0.001)	29.94 (0.03)	7.36 (0.005)
Oxbow Channel	7.6 (0.5)	42 (1)	2.7 (0.1)	12.1 (0.5)	10.3 (0.2)	9.9 (0.1)	0.96 (0.03)	0.228 (0.004)	0.226 (0.0014)	0.316 (0.001)	26.36 (0.03)	7.19 (0.01)

Values in parentheses () represent standard deviations for triplicate measurements except for %S and solid Mn and Fe content, where absolute error is reported.
[a] Phenol oxidative potential with and without added H_2O_2 performed on soil slurries.

ICP-OES, which was roughly 2 mg L^{-1} Fe and 0.4 mg L^{-1} Mn. Mn(III) was added to 125 mL soil slurries as 1.25 mL from a 40 mg Mn L^{-1}, 100x stock composed of Mn(III) acetate dihydrate (Sigma Aldrich) in sodium acetate buffer. Fe(II) was added to 125 mL soil slurries as 1.25 mL from a 200 mg Fe L^{-1}, 100x stock composed of $FeCl_2$ (Sigma Aldrich) in 2% HCl. While Mn(II) is the substrate of microbial oxidative enzymes, Mn (III) is the active oxidant produced by those enzymes, so it was chosen to represent both biological and abiotic Mn-driven contribution to oxidative potential. We assumed that both Fe(III) and Mn(III) would be actively recycled through dissimilatory reduction and Fenton or enzymatic oxidation in the L-DOPA assays, where oxygen diffusion would be limited in the standing 96-well plates, if those microbial communities were present and performing a similar role in the native soils (which the presence of Fe(II) would suggest is likely).

An autoclave treatment was chosen to sterilize samples, where remaining activity would be due to abiotic, likely metal-mediated, processes. Soils were massed into borosilicate glass serum vials in an anoxic glovebag, sealed with butyl septa, and crimped. Samples were autoclaved at 121 °C for 15 min, cooled to room temperature in the dark, and then mixed with sodium acetate buffer into soil slurries as described above and immediately used in assays. Autoclaving risks altering organic matter chemistry and increasing extractable, microbially-accessible redox-active metals (Wolf and Skipper, 1994). Utilization of L-DOPA as substrate in oxidative potential assays relieves the need to preserve native SOC chemistry. Acid-extractable and soil slurry Mn and Fe concentrations were not significantly different after autoclave sterilization, suggesting bioavailability of redox-active minerals was not greatly affected.

2.4. Statistical analysis

The effects of metal addition, H_2O_2 addition, and autoclave sterilization on oxidative potential were tested using paired Wilcoxon tests with Holm-adjusted P values to correct for multiple comparisons. The non-parametric T-test was chosen to accommodate non-normal data distributions and pairwise comparison was done to account for the soils from different hydrologic settings likely having inherently different sensitivities to experimental perturbations. Pearson correlations were performed to relate potential oxidative activity with and without added H_2O_2 to potential geochemical and microbial soil features and to relate soil organic carbon content to other soil features. Correlations were performed for both 2017 and 2020 sampling years, but the main text focuses on 2017 data because findings were similar between years and fungal sequencing data was only collected for the 2017 soils. Metal addition experiments were performed on the 2020 soils, which were collected fresh for the purpose of rapidly (~2 weeks) performing the oxidative potential assays prior to redox and microbial community shift during soil storage to further explore oxidative potential with added metals. Statistical analyses were performed in RStudio running R version 4.1.0.

3. Results

3.1. Soil characteristics

Soil Mn content did not vary consistently in 2020 samples (Table 1), although 2017 soils showed lower Mn in the wetland (~0.089–0.108 g kg^{-1}) with higher values ranging from 0.203 to 0.342 g kg^{-1} in the oxbow and meander and spuriously high (1.318 g kg^{-1}) Mn in MZT2 63–78 cm (Table S1). Extractable Mn was slightly higher in the oxbow than in the meander and was lowest at intermediate depths in the mid-meander core (Tables 1 and S1). Soil Fe content was 80- to 100-fold higher than Mn content on a soil mass basis. Fe was lowest in the wetland at ~19 g kg^{-1} and higher (~22–33 g kg^{-1}) but with no clear patterns in the oxbow and meander soils (Tables 1 and S1). Iron oxides had a similar composition across soils on the basis of Fe EXAFS analysis,

although the oxbow samples had distinct features indicative of more reduced Fe (Table S2). Acid extracts showed highest Fe content in surface meander and oxbow soils. Oxbow channel and wetland soils had almost completely reduced Fe_{HCl} (Tables 1 and S1).

Organic carbon content declined with depth in the meander soils from 3.6 to 0.4% in the mid-meander and 2.2 to 1.7% near the river, whereas oxbows and wetlands had roughly 2.5% SOC (Table 1). The C_{org}/N ratio largely mirrored SOC content and ranged from 15.2 to 7.2 in MZT2 soils, with MZT1 and oxbow soils ranging between 12.6 and 10.7 (Table 1, Fig. 5).

3.2. Fungal community analysis

DNA sequences for Basidiomycota and Ascomycota, the two fungal phyla containing white and brown rot fungi capable of producing the oxidative extracellular enzymes and ROS that degrade plant litter, were relatively less abundant in permanently saturated than seasonally saturated soils (51% vs. 91% Basidiomycota + Ascomycota fungi in permanently vs. seasonally saturated soils, respectively, T-test P = 0.001; Fig. 2). ECM fungi relative abundance was also lower in the permanently saturated soils than in the meander soils (28% vs. 56%, respectively, T-test P = 0.007; Fig. 2). Saprotroph and white rot relative abundance did not differ between the meander and oxbow soils (25% vs 26% for saprotrophs, and white rot negligible overall; Fig. 2). It is possible that absolute abundance of fungal guilds differed across soils if total fungal biomass varied, possibly overshadowing inferences made using relative abundance. Even so, relative abundance of fungal guilds represents the successful metabolisms in a given soil and thus offers clues to their ecological role when compared across soils.

Estimated richness of saprotrophs and ECM was highest in the meander near the river and in surface soils, whereas overall fungal richness was generally higher in the flooded sites – predominantly due to taxa not known for SOC depolymerization from the phyla Mortierellomycota, Chytridiomycota, and unclassified phyla (Fig. 2, Table S6).

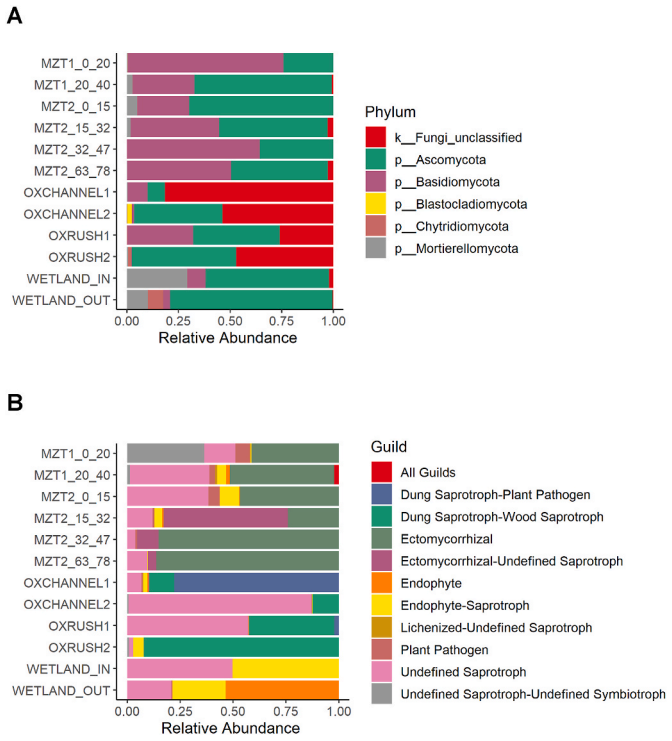

Fig. 2. Relative abundance of fungal phyla (A) and guilds (B) from ITS2 sequencing representing more than 0.1% relative abundance across samples. "All Guilds" refers to taxa assigned to saprotroph, parasite, and ecto or endomycorrhiza. "k_" and "p_" indicate kingdom and phylum, respectively.

The diversity of fungi as a whole and of saprotrophs separately was highest in the oxbow soils and mid-meander surface soil, respectively (Table S6). ECM diversity was highest in the near-river site and the mid-meander surface soils (Table S6).

3.3. Phenol oxidative potential

3.3.1. Unamended assays

Across all soils and treatments, phenol oxidative potential with added H_2O_2 ($+H_2O_2$) was significantly higher than without H_2O_2 ($-H_2O_2$) (Tables 1 and S1). In unamended, unautoclaved soils, phenol oxidative potential hovered between 1 and 2 μmol g^{-1} h^{-1} while oxidative potential $+H_2O_2$ ranged from 2 to 9 μmol g^{-1} h^{-1} (Table 1, Fig. 3). The oxbow channel had much higher oxidative potential around ~8 μmol g^{-1} h^{-1} $-H_2O_2$ and 42 μmol g^{-1} h^{-1} $+H_2O_2$ (Fig. 3; 2017 soils showed similar trends, Table S1).

3.3.2. Metal addition assays

We tested the influence of Fe(II) and Mn(III) on both enzyme-

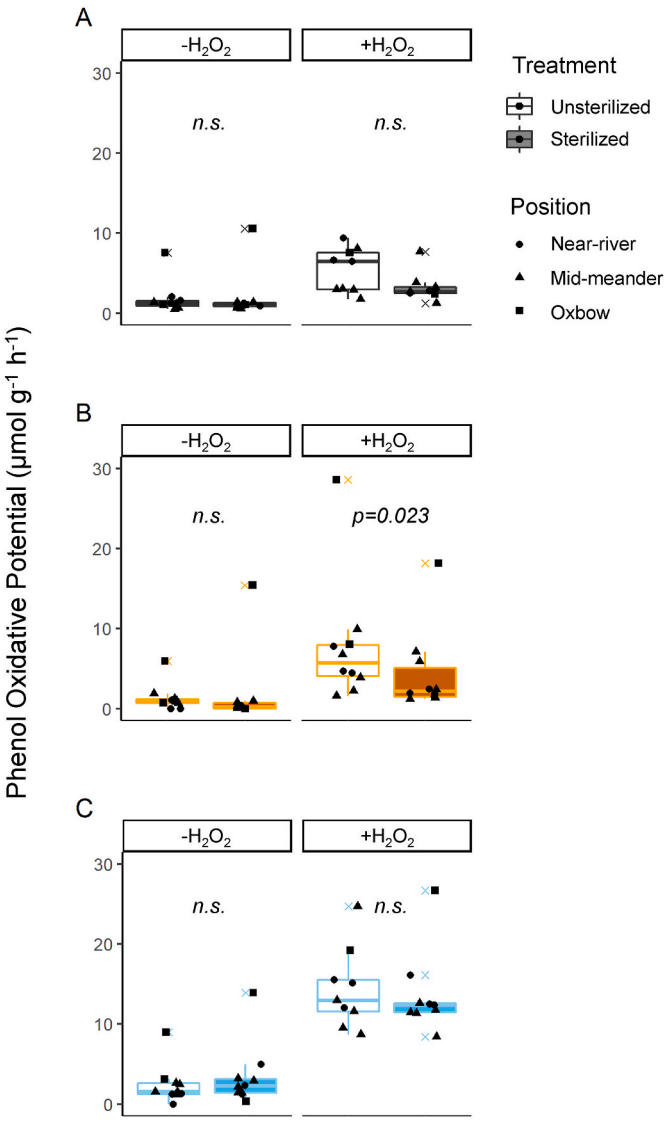

Fig. 3. Phenol oxidative potential in unamended (A), Mn(III)-amended (B) and Fe(II)-amended soils (C). The P values in subpanels describe Wilcoxon rank paired *t*-test significance for the sterilization treatment. Boxplots show median and interquartile values with x marking outliers. More detailed *t*-test outcomes are described in Tables S3–S5.

mediated (un-autoclaved) and abiotic (autoclaved) phenol oxidative potential by amending soils in L-DOPA assays with each metal at concentrations found in field soils. If native acid-extractable Mn or Fe affect phenol oxidative potential, then these metal additions should produce a similar magnitude increase in the L-DOPA assay signal to what they contribute in the unamended assay. The addition of Fe(II), but not Mn (III), increased phenol oxidative potential $+H_2O_2$ relative to unamended soils (Fig. 3, Table S5; note the marginal significance in the cases of Fe (II) vs. no added metal). The addition of either Fe or Mn did not significantly increase $–H_2O_2$ oxidative potential relative to unamended soil (Table S5).

3.3.3. Sterile vs. native activity assays

Autoclave sterilization was used to inactivate microbial enzymes, thus isolating abiotic phenol oxidative pathways relative to the unsterilized soils. Autoclave sterilization appeared to lower oxidative potential for all but the +Fe(II) $–H_2O_2$ assay (Fig. 3), but this difference was only significant in the +Mn(III) $+H_2O_2$ assay (Table S4). In unamended soils, $+H_2O_2$ oxidative potential was higher than $–H_2O_2$ oxidative potential only for the unautoclaved assays (Fig. 3, Table S3). Soil environment appeared to drive whether oxidative potential declines after autoclaving: while autoclave sterilization did not reduce oxidative activity in unamended soils overall with or without peroxide additions, the oxbow rush and near-river meander samples lost oxidative potential after sterilization in $+H_2O_2$ assays (Fig. 3 and S5). In the +Mn(III) $+H_2O_2$ treatment ostensibly targeting Mn-peroxidase and other extracellular oxidative enzyme activity, autoclave sterilization significantly reduced phenol oxidative potential.

3.4. Soil features driving SOC cycling

3.4.1. Oxidative potential correlations

The contribution of fungal enzymes versus abiotic chemical pathways to phenol degradation was explored through correlations between oxidative potential and geochemical factors or fungal community composition. Organic carbon, despite being an extracellular oxidative enzyme substrate, was not significantly related to phenol oxidative potential $–H_2O_2$ (Table 2, Fig. S2). SOC did correlate to $+H_2O_2$ phenol oxidative potential in the 2020 soils with the oxbow outlier removed, but not in the 2017 soils (Tables 2 and S1; Fig. 4 and S2). Soil organic nitrogen (SON) modestly correlated with phenol oxidative activity $+H_2O_2$ (Table 2).

Acid-extractable Fe, both total and Fe(II), was positively correlated to oxidative potential $–H_2O_2$ ($r = 0.78$, $P = 0.003$ and $r = 0.85$, $P < 0.001$, Fe(total) and Fe(II) respectively; Table 2) and $+H_2O_2$ ($r = 0.76$, $P = 0.004$ and $r = 0.78$, $P = 0.003$ for 2017 correlations, Table 2; 2020 soils had stronger relationships, Fig. 4). Peroxidative activity was less strongly correlated with $Fe(II)/Fe(total)_{HCl}$ than with $Fe(II)_{HCl}$ or $Fe(total)_{HCl}$ (Table 2, Fig. 4), though $Fe(II)/Fe(total)_{HCl}$ correlated strongly with oxidative potential in drier meander soils (Fig. S1). Acid-extractable Mn somewhat explained phenol oxidative potential after removing the oxbow outlier (Fig. 4), but in 2017 Mn_{HCl} showed no meaningful variation across soils or relationship to phenol oxidative potential (Tables 1 and 2).

Overall fungal and BA diversity were significantly correlated with oxidative potential $–H_2O_2$ ($r = 0.65$, $P = 0.021$ and $r = 0.68$, $P = 0.016$ for all fungi and BA respectively) and $+H_2O_2$ ($r = 0.63$, $P = 0.029$ and $r = 0.62$, $P = 0.031$ for fungi and BA respectively; Table 2). However, the guilds known for phenol oxidation – ECM and saprotrophs – were not correlated to phenol oxidative potential with or without H_2O_2, and BA relative abundance was anti-correlated with $–H_2O_2$ phenol oxidative potential ($r = -0.59$, $P = 0.042$; Table 2). Fungal community showed correlations with acid-extractable Fe, where fungal diversity was positively correlated with $Fe(total)_{HCl}$ and BA relative abundance negatively correlated with $Fe(total)_{HCl}$ (Table 2).

3.4.2. Soil organic carbon correlations

Correlations of soil fungal community composition metrics and geochemical factors were performed vs. SOC to explore possible SOC protection mechanisms competing with oxidative loss in these floodplain soils. In a comparison of acid-extractable Fe versus SOC, permanently flooded soils – particularly the channel in 2020 – had higher $Fe(II)/Fe(total)_{HCl}$, $Fe(II)_{HCl}$, and $Fe(total)_{HCl}$ relative to meander soils, so much so in the case of Fe(II) as to render the SOC vs. $Fe(II)_{HCl}$ correlation insignificant (Fig. 5, S3). In contrast, permanently flooded soils were not outliers in comparisons of SOC with soil features unrelated to redox

Table 2
Pearson correlation coefficients and P-values for possible geochemical and fungal drivers of phenol oxidative potential and soil organic carbon distribution in 2017 soils. Significant differences at $\alpha = 0.05$ are indicated in bold. Significance levels: *P < 0.05, **P < 0.01, ***P < 0.001.

	Phenol Oxidative Potential $–H_2O_2$		Phenol Oxidative Potential $+H_2O_2$		SOC		$Fe(total)_{HCl}$	
	r	P	r	P	r	P	r	P
Total C	0.43	0.17	**0.59**	*	**0.97**	***	**0.70**	*
Total N	0.27	0.39	0.50	0.10	**0.89**	***	0.48	0.11
SOC	0.32	0.31	0.51	0.09	NA	NA	**0.64**	*
SON	0.46	0.14	**0.62**	*	**0.70**	*	**0.75**	**
C_{org}/N	0.27	0.40	0.29	0.37	**0.69**	*	**0.62**	*
Mn_{HCl}	0.46	0.13	0.41	0.18	0.26	0.42	**0.70**	*
Mn Total	−0.12	0.71	−0.14	0.67	−0.32	0.31	−0.08	0.79
$Fe(II)_{HCl}$	**0.85**	***	**0.78**	**	0.57	0.05	**0.95**	***
$Fe(total)_{HCl}$	**0.78**	**	**0.76**	**	**0.64**	*	NA	NA
$Fe(II)/Fe(total)_{HCl}$	0.48	0.11	0.47	0.12	0.45	0.14	0.52	0.08
Fe Total	0.20	0.53	0.20	0.53	−0.16	0.61	0.26	0.41
Fungal Richness	0.28	0.37	0.25	0.44	−0.28	0.37	−0.04	0.90
Fungal Diversity	**0.65**	*	**0.63**	*	0.47	0.12	**0.77**	**
BA Rel. Abund.	**−0.59**	*	−0.38	0.23	−0.17	0.60	**−0.67**	*
BA Richness	−0.25	0.44	−0.09	0.78	0.33	0.30	−0.10	0.76
BA Diversity	**0.68**	*	**0.62**	*	0.43	0.16	0.54	0.07
Sap. Rel. Abund.	0.00	0.99	0.16	0.62	−0.36	0.26	−0.19	0.56
Sap. Richness	−0.20	0.53	−0.04	0.89	0.38	0.23	−0.04	0.91
Sap. Diversity	−0.05	0.89	0.01	0.98	0.27	0.40	−0.05	0.87
ECM Rel. Abund.	−0.32	0.32	−0.04	0.91	−0.09	0.79	−0.44	0.15
ECM Richness	−0.24	0.46	−0.08	0.80	0.32	0.31	−0.15	0.64
ECM Diversity	0.00	1.00	0.26	0.42	0.50	0.10	0.06	0.86
White Rot Rel. Abund.	−0.27	0.40	−0.34	0.27	−0.19	0.55	−0.23	0.48
White Rot Richness	−0.11	0.74	0.10	0.76	**0.76**	*	0.16	0.61
White Rot Diversity	−0.16	0.63	0.06	0.86	**0.73**	**	0.07	0.84

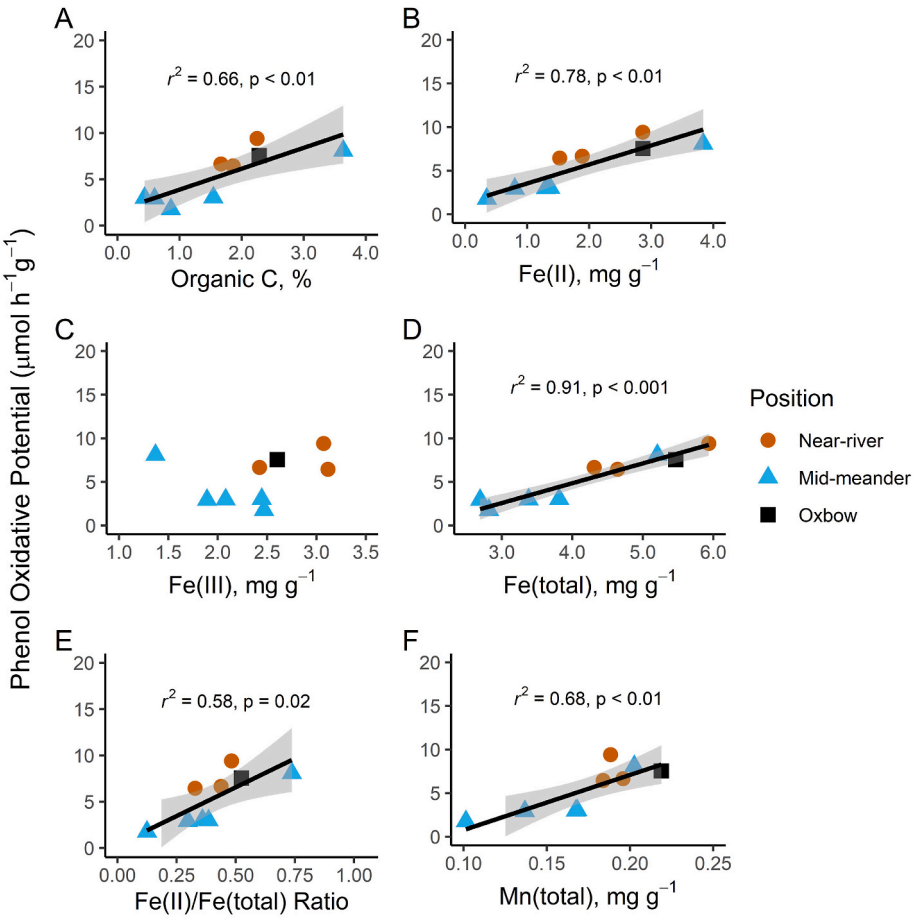

Fig. 4. Relationship between phenol oxidative potential with added H_2O_2 and soil geochemical parameters related to oxidative activity for soils collected in 2020 with an outlying oxbow sample removed. Trend lines show significant linear relationships with phenol oxidative potential + H_2O_2.

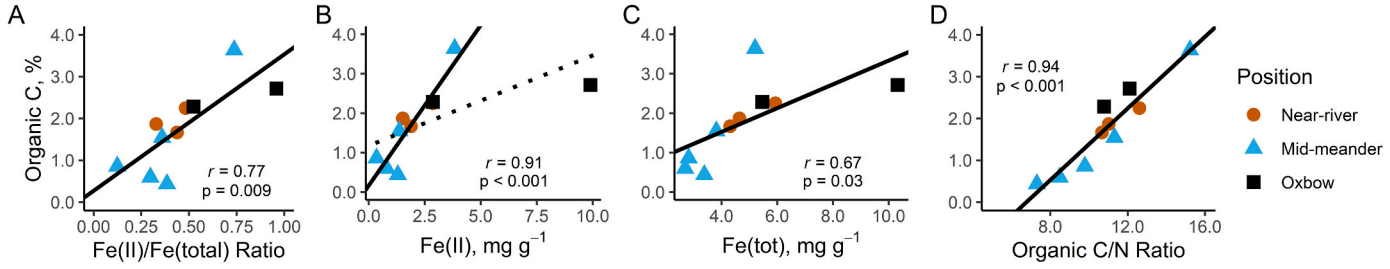

Fig. 5. Relationship between SOC (%) and soil geochemical parameters related to oxidation activity for soils collected in 2020. Pearson correlation trends and statistics are shown between SOC and Fe(II)/Fe(total)$_{HCl}$ (A), Fe(II)$_{HCl}$ (B), Fe(total)$_{HCl}$ (C), and C_{org}/N (D) with solid trendlines. The dotted line represents a marginally significant relationship (P = 0.05) prior to removing the outlying oxbow channel sample.

status such as C_{org}/N (Fig. 5, S3). Of the fungal parameters measured, SOC was only significantly correlated with white rot richness and diversity (r = 0.76, P = 0.004 and r = 0.73, P = 0.007, respectively; Table 2).

4. Discussion

4.1. Microbial drivers of oxidative activity

Recent findings of the importance of Fe and Mn in organic matter oxidation in wetlands or frequently saturated soils prompted us to look at the drivers of phenol oxidative potential along floodplain soils ranging in water residence time and redox-active metal availability. We found that meander topsoils and permanently flooded soils had the highest phenol oxidative potential. Relative to deep meander soils, these surface soils had higher organic carbon content. Soil phenol oxidative potential commonly increases with organic carbon content, particularly the abundance of phenolic substrates (Aber et al., 1990; Sinsabaugh and Moorhead, 1994). Inversely, litter mass loss often corresponds to oxidative enzyme activity (Sinsabaugh et al., 1992; Allison and Vitousek, 2004). However, we did not observe a significant relationship between oxidative potential with or without H_2O_2 and organic carbon concentration or quality (C_{org}/N), suggesting polyphenolic substrate concentration does not drive oxidation potential here. Moreover, the microorganisms that degrade litter and whose diversity reflects soil organic matter content and quality unlikely exclusively drive its degradation in these soils.

Oxidative enzymes require molecular oxygen and thus their

secretion should depend on factors controlling oxygen supply and demand, but the high oxidative potential in our flooded oxbow soils precluded oxygen availability from controlling phenol oxidative potential at our site. This is counter to the many site-specific studies that have shown higher phenol oxidase and peroxidase activity during periods of drainage of wetland soils (Sinsabaugh et al., 1992; Fenner and Freeman, 2011; Kwon et al., 2013). In these studies, higher oxidative activity upon drainage is attributed to oxygen availability for extracellular oxidative enzymes produced by diverse microbial communities. These saprotrophic communities increase oxidative enzyme production upon exposure to oxygen (Freeman et al., 2001, 2004). The typical absence of microorganisms known for producing extracellular oxidative enzymes in flooded soils – for instance, white rot fungi (Kwon et al. (2013) – and our observation of lower or similar richness and diversity of saprotrophic, ECM and white-rot guilds in permanently vs. periodically saturated soils, suggests a non-microbial driver of SOC depolymerization potential across floodplain soils.

4.2. The case for Fe(II)-mediated oxidation

Counter to the ecology of microbial oxidative degradation, we observed the highest phenol oxidative potential in the most reducing oxbow soils with the highest Fe(II)/Fe(total)$_{HCl}$ ratios and lowest field measurements of Eh and dissolved oxygen. Moreover, autoclave sterilization did not significantly reduce high phenol oxidation in the more reducing soils. Oxidative potential with and without H_2O_2 correlated significantly with Fe_{HCl}, particularly Fe(II)$_{HCl}$, and with Mn_{HCl} in 2020 (Fig. 4 and S2, Table 2).

Studies in upland soils implicate Mn redox cycling, particularly the formation of Mn(III), as a strong driver of SOC decomposition along redox gradients (Keiluweit et al., 2015; Jones et al., 2018). A positive correlation between Mn_{HCl} and SOC in the field soils suggested that active Mn redox cycling was possible and could contribute to lowland phenolics oxidation by Mn(III) (Table 2). However, Mn-mediated phenol oxidative activity seemed relatively unimportant at this field site given that Mn(III) amendment did not increase phenol oxidative potential, particularly $-H_2O_2$, across samples and years (Fig. 3, Table S5).

While +Mn and $+H_2O_2$ was the only treatment combination for which sterilization decreased L-DOPA oxidation, suggesting an active Mn-utilizing peroxidase pool and microbial recycling of Mn(III) driving floodplain phenol oxidative activity; Mn addition did not significantly increase phenol oxidative activity above unamended soils overall (Fig. 3). Mn(III) addition enhanced phenol oxidation in mid-meander soils but lowered it in near-meander soils (Figs. S4 and S5). Mid-meander microbial communities may be Mn-limited such that Mn(III) addition enhances their oxidative activity. Lower Mn_{HCl} but similar Mn (total) in the mid-meander versus near-river cores corroborates Mn limitation (Table 1). This is consistent with down-regulation of lignin peroxidase in the near-meander soils and the up-regulation of Mn-peroxidase (or coincidental Mn(II) oxidation by other fungal (per)oxidases) in the mid-meander driven by Mn additions, a pattern previously observed in both activity and RT-PCR assays with the white rot *Phanerochaete chrypsosporium* (Bonnarme and Jeffries, 1990; Gettemy et al., 1998). While microbial communities appear to utilize Mn to catalyze SOC oxidation, this activity is coincidental in all but the near-river meander soils and does not explain the far higher phenol oxidation potential in the permanently flooded or mid-meander topsoils.

Iron, by contrast, appears to consistently drive phenol oxidative potential across all soil hydrologic settings. Fe(II)$_{HCl}$, Fe(total)$_{HCl}$ and Fe (II)/Fe(total)$_{HCl}$ were all positively related to phenol oxidation with and without H_2O_2 (Table 2, Fig. 4). Therefore, the abundance of Fe, and Fe (II) in particular, rather than reducing conditions (as a relationship with only Fe(II)/Fe(total) would indicate) appeared to drive phenol oxidative potential in our soils. Fe(II) enhanced L-DOPA oxidation, regardless of sterilization treatment and H_2O_2 addition (Fig. 3, Table S5). This indicates that the metal itself rather than microbial use of Fe to catalyze Fenton reactions or as an enzyme cofactor mediates Fe-associated oxidative activity in these soils. Moreover, we found that the oxidative activity associated with Fe(II) acted on a variety of organic linkages including lower-energy bonds susceptible to phenol oxidase cleavage and higher-energy bonds susceptible to peroxidase-mediated cleavage (Datta et al., 2017), suggesting a non-selective oxidant such as ROS. Microbial and abiotic Fe(II)-catalyzed reactions likely both contribute to native floodplain SOC oxidative degradation, resulting in a significant potential for Fe(II) to enhance phenol oxidative activity in redox hotspots throughout permanently and temporarily flooded wetland soils.

Abiotic influences on apparent phenol oxidative activity have been observed in *Sphagnum* peat soils, where a lowered water table decreases measured phenol oxidase activity (L-DOPA oxidation $-H_2O_2$), but peat oxidation was still observed (Xiang et al., 2013). Other studies of pure phenol oxidases, coastal dune sediments, arctic surface waters, and alpine wetland soils (Van Bodegom et al., 2005; Page et al., 2013; Wang et al., 2017) associate increased phenol oxidative activity with Fe(II), implicating a Fenton-like mechanism with corresponding measurements of •OH (Trusiak et al., 2018). Within these studies, iron (both reduced and oxidized due to rapid microbial dissimilatory Fe(III) reduction) plays a major role in modifying phenol oxidative activity and phenolic degradation. In Arctic surface waters, Fenton chemistry is calculated to produce CO_2 at rates similar to microbial oxidation (Page et al., 2013). Moreover, Yuan et al. (2022) found 6–80 nM H_2O_2 in a more reducing nearby East River meander and cutoff oxbow sediments, confirming the likelihood of H_2O_2 being consistently available at our field site. Floodplains experience dynamic oxygen and Fe(II) supply to high-carbon surface soils, making them prime locations for Fenton-mediated SOC oxidation. This pool of reactive iron may significantly enhance mountainous floodplain SOC loss under climate-related hydrologic change as summer monsoon precipitation pulses combine with generally drier conditions from reduced snowpack.

4.3. Implications for floodplain organic carbon

While Fe promotes organic carbon loss through abiotic depolymerization, it can also enhance SOC storage. Strong relationships between SOC and Fe across our site suggested that Fe might contribute to carbon storage in these floodplain soils through several hypothesized processes. Soils with both higher total Fe_{HCl} and a higher fraction of Fe(II)$_{HCl}$ tended to have the greatest SOC. Many studies have shown that reducing conditions, and particularly high Fe(II)/Fe(total)$_{HCl}$, are associated with increased carbon storage (Page et al., 2011; Mitsch et al., 2013; Boye et al., 2017). Anaerobic conditions enhance SOC storage through energetic limitations on anaerobic microbial metabolisms including dissimilatory sulfate and iron reduction (Boye et al., 2017; Keiluweit et al., 2017; Bhattacharyya et al., 2018; Naughton et al., 2021). However, Fe (II) at an active redox interface may not necessarily correspond to consistently low redox potential and anoxia, and thus SOC energetic preservation potential. Variably saturated environments promote high Fe(II) production rates up to roughly 10% of total Fe per day (Calabrese et al., 2020). Fluctuating or heterogeneous redox conditions, such as those observed in the oxbow and meander surface soils and indicated by high Fe(II)$_{HCl}$, likely affect SOC stocks through opposing Fe(II)-driven oxidative depolymerization and preservation via poor microbial energetics.

Alternatively, Fe(total)$_{HCl}$ – which represents high surface area, reactive iron oxides such as ferrihydrite and lepidocrocite, as well as surface-sorbed iron (Poulton and Canfield, 2005) – could be associated with SOC through co-precipitation and sorption (Faust et al., 2021; Jeewani et al., 2021). In the meander soils, high Fe(total)$_{HCl}$ likely contributes to high SOC concentrations through the formation of mineral-associated organic matter, particularly short-range order Fe (III)-hydroxides. These associations could form with Fe(II) oxidized after flooding and in the presence of C inputs from plant roots (Chen and Thompson, 2021) or from allochthonous Fe sources from upstream or

hyporheic flows (Herndon et al., 2017). It is also possible that Fe(II) oxidative activity contributes to the oxidative degradation of shale in the East River floodplain substratum, releasing organic carbon that can then associate with soil minerals, given the estimated near-third of SOC derived from shale in a nearby meander (Fox et al., 2020).

Factors unrelated to Fe(II) content, such as microbial activity and carbon inputs, could also explain the apparent relationships between Fe and SOC. High-iron and high-carbon topsoils, both permanently and seasonally flooded, also likely have high inputs from plant exudates and litter as indicated by higher C_{org}/N ratios (Table 1). More active surface soil microbial communities could also integrate plant-derived carbon into mineral-stabilized carbon more effectively than in subsoils (Sokol et al., 2019). Even so, correlations indicate two distinct trends in SOC protection mechanisms across floodplain zones: one associated with high total Fe in seasonally flooded soils, and one associated with poor redox energetics that is counteracted by Fenton-type reactions in permanently flooded (e.g., oxbow) soils.

While this work fits into the growing framework of evidence for Fe (II)-driven oxidative degradation of organic matter in reducing soils and aquatic environments, its novelty is the comparison between permanently and seasonally saturated soils within a floodplain environment. In a clear divergence from upland, forested soils (Allison et al., 2009; Keiluweit et al., 2015; Talbot et al., 2015; Entwistle et al., 2018; Jones et al., 2018), Fe content rather than Mn or microbial oxidative activity predominantly drove phenol oxidation potential in these frequently saturated floodplain soils. Total Fe was just as significant a predictor of oxidative activity as Fe(II), suggesting the potential for rapid microbial Fe reduction in an autocatalytic cycle producing ROS through a chain of Fenton reactions (Hall and Silver, 2013; Ginn et al., 2017). Such processes possibly counteract SOC retention through mineral association in frequently flooded soils. Moreover, we show here the need to consider Fe-mediated organic matter oxidation in both reducing soils and aerobic soils with a history of flooding. Future models of wetland (whether permanent or seasonal) SOC cycling should therefore consider abiotic depolymerization and oxidation processes in order to accurately represent wetland potential for carbon storage and carbon dioxide release.

Declaration of competing interest

The authors declare that they have no known competing financial interests or personal relationships that could have appeared to influence the work reported in this paper.

Data availability

Data and code will be made available on request and on GitHub: https://github.com/hrnaughton/MetalvsFungalOxidation.

Acknowledgements

This work was performed with support from the U.S. Department of Energy, Office of Science through the Office of Biological and Environmental Research, Environmental System Science Program [Award Number DE-SC0016544]; Facilities Integrating Collaborations for User Science [FICUS User Proposal 49518] program in collaboration with the Environmental and Molecular Sciences Laboratory (Richland, WA) and Joint Genome Institute (Berkeley, CA); and the Watershed Function Scientific Focus Area funded by the U.S. Department of Energy, Office of Science, Office of Biological and Environmental Research [Contract No. DE-AC02-05CH11231]. We thank Lizzie Paulus and Ted Raab for help in developing the enzyme assay protocol and our East River collaborators Cam Anderson, Patricia Fox, Markus Kleber, Shawn Benner and Sam Pierce for help in the field. We also appreciate Juan Lezama-Pacheco, Doug Turner and Guangchao Li for providing instrument access and analysis assistance with geochemical data. The authors declare no conflict of interest.

Appendix A. Supplementary data

Supplementary data to this article can be found online at https://doi.org/10.1016/j.soilbio.2023.108962.

References

Aber, J.D., Melillo, J.M., McClaugherty, C.A., 1990. Predicting long-term patterns of mass loss, nitrogen dynamics, and soil organic matter formation from initial fine litter chemistry in temperate forest ecosystems. Canadian Journal of Botany 68, 2201–2208. https://doi.org/10.1139/b90-287.

Aguirre, J., Ríos-Momberg, M., Hewitt, D., Hansberg, W., 2005. Reactive oxygen species and development in microbial eukaryotes. Trends in Microbiology 13, 111–118. https://doi.org/10.1016/j.tim.2005.01.007.

Allison, S.D., LeBauer, D.S., Ofrecio, M.R., Reyes, R., Ta, A.-M., Tran, T.M., 2009. Low levels of nitrogen addition stimulate decomposition by boreal forest fungi. Soil Biology and Biochemistry 41, 293–302. https://doi.org/10.1016/j.soilbio.2008.10.032.

Allison, S.D., Vitousek, P.M., 2004. Extracellular enzyme activities and carbon chemistry as drivers of tropical plant litter decomposition. Biotropica 36, 285–296. https://doi.org/10.1111/j.1744-7429.2004.tb00321.x.

Bach, C.E., Warnock, D.D., Van Horn, D.J., Weintraub, M.N., Sinsabaugh, R.L., Allison, S.D., German, D.P., 2013. Measuring phenol oxidase and peroxidase activities with pyrogallol, l-DOPA, and ABTS: effect of assay conditions and soil type. Soil Biology and Biochemistry 67, 183–191. https://doi.org/10.1016/j.soilbio.2013.08.022.

Bhattacharyya, A., Campbell, A.N., Tfaily, M.M., Lin, Y., Silver, W.L., Nico, P.S., Pett-Ridge, J., 2018. Redox fluctuations control the coupled cycling of iron and carbon in tropical forest soils. Environmental Science & Technology 52, 14129–14139. https://doi.org/10.1101/312108.

Blanchette, R.A., W. Krueger, E., Haight, J.E., Akhtar, Masood, Akin, D.E., 1997. Cell wall alterations in loblolly pine wood decayed by the white-rot fungus, *Ceriporiopsis subvermispora*. Journal of Biotechnology 53, 203–213. https://doi.org/10.1016/S0168-1656(97)01674-X.

Bonnarme, P., Jeffries, T.W., 1990. Mn(II) regulation of lignin peroxidases and manganese-dependent peroxidases from lignin-degrading white rot fungi. Applied and Environmental Microbiology 56, 210–217. https://doi.org/10.1128/aem.56.1.210-217.1990.

Boye, K., Noël, V., Tfaily, M.M., Bone, S.E., Williams, K.H., Bargar, J.R., Fendorf, S., 2017. Thermodynamically controlled preservation of organic carbon in floodplains. Nature Geoscience 10, 415–419. https://doi.org/10.1038/ngeo2940.

Bridgham, S.D., Megonigal, J.P., Keller, J.K., Bliss, N.B., Trettin, C., 2006. The carbon balance of North American wetlands. Wetlands 26, 889–916. https://doi.org/10.1672/0277-5212(2006)26[889:TCBONA]2.0.CO;2.

Bugg, T.D.H., Ahmad, M., Hardiman, E.M., Rahmanpour, R., 2011. Pathways for degradation of lignin in bacteria and fungi. Natural Product Reports 28, 1883–1896. https://doi.org/10.1039/C1NP00042J.

Calabrese, S., Barcellos, D., Thompson, A., Porporato, A., 2020. Theoretical constraints on Fe reduction rates in upland soils as a function of hydroclimatic conditions. Journal of Geophysical Research: Biogeosciences 125, e2020JG005894. https://doi.org/10.1029/2020JG005894.

Chen, C., Thompson, A., 2021. The influence of native soil organic matter and minerals on ferrous iron oxidation. Geochimica et Cosmochimica Acta 292, 254–270. https://doi.org/10.1016/j.gca.2020.10.002.

Datta, R., Kelkar, A., Baraniya, D., Molaei, A., Moulick, A., Meena, R.S., Formanek, P., 2017. Enzymatic degradation of lignin in soil: a review. Sustainability 9, 1163. https://doi.org/10.3390/su9071163.

DeForest, J.L., 2009. The influence of time, storage temperature, and substrate age on potential soil enzyme activity in acidic forest soils using MUB-linked substrates and l-DOPA. Soil Biology and Biochemistry 41, 1180–1186. https://doi.org/10.1016/j.soilbio.2009.02.029.

Diaz, J.M., Hansel, C.M., Voelker, B.M., Mendes, C.M., Andeer, P.F., Zhang, T., 2013. Widespread production of extracellular superoxide by heterotrophic bacteria. Science 340, 1223–1226. https://doi.org/10.1126/science.1237331.

Dubinsky, E.A., Silver, W.L., Firestone, M.K., 2010. Tropical forest soil microbial communities couple iron and carbon biogeochemistry. Ecology 91, 2604–2612. https://doi.org/10.1890/09-1365.1.

Eastwood, D.C., Floudas, D., Binder, M., Majcherczyk, A., Schneider, P., Aerts, A., Asiegbu, F.O., Baker, S.E., Barry, K., Bendiksby, M., Blumentritt, M., Coutinho, P.M., Cullen, D., Vries, R.P. de, Gathman, A., Goodell, B., Henrissat, B., Ihrmark, K., Kauserud, H., Kohler, A., LaButti, K., Lapidus, A., Lavin, J.L., Lee, Y.-H., Lindquist, E., Lilly, W., Lucas, S., Morin, E., Murat, C., Oguiza, J.A., Park, J., Pisabarro, A.G., Riley, R., Rosling, A., Salamov, A., Schmidt, O., Schmutz, J., Skrede, I., Stenlid, J., Wiebenga, A., Xie, X., Kües, U., Hibbett, D.S., Hoffmeister, D., Högberg, N., Martin, F., Grigoriev, I.V., Watkinson, S.C., 2011. The plant cell wall–decomposing machinery underlies the functional diversity of forest fungi. Science 333, 762–765. https://doi.org/10.1126/science.1205411.

Entwistle, E.M., Romanowicz, K.J., Argiroff, W.A., Freedman, Z.B., Morris, J.J., Zak, D.R., 2018. Anthropogenic N deposition alters the composition of expressed class II fungal peroxidases. Applied and Environmental Microbiology 84, e02816-e02817. https://doi.org/10.1128/AEM.02816-17.

Faust, J.C., Tessin, A., Fisher, B.J., Zindorf, M., Papadaki, S., Hendry, K.R., Doyle, K.A., März, C., 2021. Millennial scale persistence of organic carbon bound to iron in Arctic marine sediments. Nature Communications 12, 275. https://doi.org/10.1038/s41467-020-20550-0.

Fenner, N., Freeman, C., 2011. Drought-induced carbon loss in peatlands. Nature Geoscience 4, 895–900. https://doi.org/10.1038/ngeo1323.

Flournoy, D.S., Kirk, T.K., Highley, T.L., 1991. Wood decay by brown-rot fungi : changes in pore structure and cell wall volume. Oct. 1991 Holzforschung 45 (5), 383–388.

Fontaine, S., Barot, S., 2005. Size and functional diversity of microbe populations control plant persistence and long-term soil carbon accumulation. Ecology Letters 8, 1075–1087. https://doi.org/10.1111/j.1461-0248.2005.00813.x.

Fox, P.M., Bill, M., Heckman, K., Conrad, M., Anderson, C., Keiluweit, M., Nico, P.S., 2020. Shale as a source of organic carbon in floodplain sediments of a mountainous watershed. Journal of Geophysical Research: Biogeosciences 125, e2019JG005419. https://doi.org/10.1029/2019JG005419.

Freeman, C., Ostle, N., Kang, H., 2001. An enzymic "latch" on a global carbon store. Nature 409. https://doi.org/10.1038/35051650, 149–149.

Freeman, C., Ostle, N.J., Fenner, N., Kang, H., 2004. A regulatory role for phenol oxidase during decomposition in peatlands. Soil Biology and Biochemistry, Enzymes in the Environment: Activity, Ecology and Applications 36, 1663–1667. https://doi.org/10.1016/j.soilbio.2004.07.012.

Gardes, M., Bruns, T.D., 1993. ITS primers with enhanced specificity for basidiomycetes - application to the identification of mycorrhizae and rusts. Molecular Ecology 2, 113–118. https://doi.org/10.1111/j.1365-294X.1993.tb00005.x.

German, D.P., Weintraub, M.N., Grandy, A.S., Lauber, C.L., Rinkes, Z.L., Allison, S.D., 2011. Optimization of hydrolytic and oxidative enzyme methods for ecosystem studies. Soil Biology and Biochemistry 43, 1387–1397. https://doi.org/10.1016/j.soilbio.2011.03.017.

Gettemy, J.M., Ma, B., Alic, M., Gold, M.H., 1998. Reverse transcription-PCR analysis of the regulation of the manganese peroxidase gene family. Applied and Environmental Microbiology 64, 569–574. https://doi.org/10.1128/AEM.64.2.569-574.1998.

Ginn, B., Meile, C., Wilmoth, J., Tang, Y., Thompson, A., 2017. Rapid iron reduction rates are stimulated by high-amplitude redox fluctuations in a tropical forest soil. Environmental Science & Technology 51, 3250–3259. https://doi.org/10.1021/acs.est.6b05709.

Gómez-Toribio, V., Martínez, A.T., Martínez, M.J., Guillén, F., 2001. Oxidation of hydroquinones by the versatile ligninolytic peroxidase from Pleurotus eryngii. European Journal of Biochemistry 268, 4787–4793. https://doi.org/10.1046/j.1432-1327.2001.02405.x.

Hall, S.J., Silver, W.L., 2013. Iron oxidation stimulates organic matter decomposition in humid tropical forest soils. Global Change Biology 19, 2804–2813. https://doi.org/10.1111/gcb.12229.

Han, R., Lv, J., Huang, Z., Zhang, Suhuan, Zhang, Shuzhen, 2019. Pathway for the Production of Hydroxyl Radicals during the Microbially Mediated Redox Transformation of Iron (Oxyhydr)oxides. Environmental Science & Technology. https://doi.org/10.1021/acs.est.9b06220.

Herndon, E., AlBashaireh, A., Singer, D., Roy Chowdhury, T., Gu, B., Graham, D., 2017. Influence of iron redox cycling on organo-mineral associations in Arctic tundra soil. Geochimica et Cosmochimica Acta 207, 210–231. https://doi.org/10.1016/j.gca.2017.02.034.

Hofrichter, M., 2002. Review: lignin conversion by manganese peroxidase (MnP). Enzyme and Microbial Technology 30, 454–466. https://doi.org/10.1016/S0141-0229(01)00528-2.

Ihrmark, K., Bödeker, I.T.M., Cruz-Martinez, K., Friberg, H., Kubartova, A., Schenck, J., Strid, Y., Stenlid, J., Brandström-Durling, M., Clemmensen, K.E., Lindahl, B.D., 2012. New primers to amplify the fungal ITS2 region – evaluation by 454-sequencing of artificial and natural communities. FEMS Microbiology Ecology 82, 666–677. https://doi.org/10.1111/j.1574-6941.2012.01437.x.

Inubushi, K., Wada, H., Takai, Y., 1984. Easily decomposable organic matter in paddy soil. Soil Science & Plant Nutrition 30, 189–198. https://doi.org/10.1080/00380768.1984.10434682.

Jackson, R.B., Lajtha, K., Crow, S.E., Hugelius, G., Kramer, M.G., Piñeiro, G., 2017. The ecology of soil carbon: pools, vulnerabilities, and biotic and abiotic controls. Annual Review of Ecology, Evolution, and Systematics 48, 419–445. https://doi.org/10.1146/annurev-ecolsys-112414-054234.

Jeewani, P.H., Van Zwieten, L., Zhu, Z., Ge, T., Guggenberger, G., Luo, Y., Xu, J., 2021. Abiotic and biotic regulation on carbon mineralization and stabilization in paddy soils along iron oxide gradients. Soil Biology and Biochemistry 160, 108312. https://doi.org/10.1016/j.soilbio.2021.108312.

Jones, M.E., LaCroix, R.E., Zeigler, J., Ying, S.C., Nico, P.S., Keiluweit, M., 2020. Enzymes, manganese, or iron? Drivers of oxidative organic matter decomposition in soils. Environmental Science & Technology 54, 14114–14123. https://doi.org/10.1021/acs.est.0c04212.

Jones, M.E., Nico, P.S., Ying, S., Regier, T., Thieme, J., Keiluweit, M., 2018. Manganese-driven carbon oxidation at oxic–anoxic interfaces. Environmental Science & Technology 52, 12349–12357. https://doi.org/10.1021/acs.est.8b03791.

Keenan, C.R., Sedlak, D.L., 2008. Factors affecting the yield of oxidants from the reaction of nanoparticulate zero-valent iron and oxygen. Environmental Science & Technology 42, 1262–1267. https://doi.org/10.1021/es7025664.

Keiluweit, M., Nico, P., Harmon, M.E., Mao, J., Pett-Ridge, J., Kleber, M., 2015. Long-term litter decomposition controlled by manganese redox cycling. Proceedings of the National Academy of Sciences 112, E5253–E5260. https://doi.org/10.1073/pnas.1508945112.

Keiluweit, M., Wanzek, T., Kleber, M., Nico, P., Fendorf, S., 2017. Anaerobic microsites have an unaccounted role in soil carbon stabilization. Nature Communications 8. https://doi.org/10.1038/s41467-017-01406-6.

Kim, D., Nakashima, T., Matsuyama, Y., Niwano, Y., Yamaguchi, K., Oda, T., 2007. Presence of the distinct systems responsible for superoxide anion and hydrogen peroxide generation in red tide phytoplankton Chattonella marina and Chattonella ovata. Journal of Plankton Research 29, 241–247. https://doi.org/10.1093/plankt/fbm011.

King, D.Whitney, Lounsbury, H.A., Millero, F.J., 1995. Rates and mechanism of Fe(II) oxidation at nanomolar total iron concentrations. Environmental Science & Technology 29, 818–824. https://doi.org/10.1021/es00003a033.

Kwon, M.J., Haraguchi, A., Kang, H., 2013. Long-term water regime differentiates changes in decomposition and microbial properties in tropical peat soils exposed to the short-term drought. Soil Biology and Biochemistry 60, 33–44. https://doi.org/10.1016/j.soilbio.2013.01.023.

Lal, R., 2008. Carbon sequestration. Philosophical Transactions of the Royal Society B: Biological Sciences 363, 815–830. https://doi.org/10.1098/rstb.2007.2185.

Lipson, D.A., Jha, M., Raab, T.K., Oechel, W.C., 2010. Reduction of iron (III) and humic substances plays a major role in anaerobic respiration in an Arctic peat soil. Journal of Geophysical Research: Biogeosciences 115, G00I06. https://doi.org/10.1029/2009JG001147.

Liptzin, D., Silver, W.L., 2009. Effects of carbon additions on iron reduction and phosphorus availability in a humid tropical forest soil. Soil Biology and Biochemistry 41, 1696–1702. https://doi.org/10.1016/j.soilbio.2009.05.013.

Luther, G.W., 2010. The role of one- and two-electron transfer reactions in forming thermodynamically unstable intermediates as barriers in multi-electron redox reactions. Aquatic Geochemistry 16, 395–420. https://doi.org/10.1007/s10498-009-9082-3.

Martinez-Villalobos, C., Neelin, J.D., 2018. Shifts in precipitation accumulation extremes during the warm season over the United States. Geophysical Research Letters 45, 8586–8595. https://doi.org/10.1029/2018GL078465.

McMurdie, P.J., Holmes, S., 2013. Phyloseq: an R package for reproducible interactive analysis and graphics of microbiome census data. PLoS One 8, e61217. https://doi.org/10.1371/journal.pone.0061217.

Millero, F.J., Sotolongo, S., 1989. The oxidation of Fe(II) with H2O2 in seawater. Geochimica et Cosmochimica Acta 53, 1867–1873. https://doi.org/10.1016/0016-7037(89)90307-4.

Minella, M., De Laurentiis, E., Maurino, V., Minero, C., Vione, D., 2015. Dark production of hydroxyl radicals by aeration of anoxic lake water. Science of The Total Environment 527–528, 322–327. https://doi.org/10.1016/j.scitotenv.2015.04.123.

Mitsch, W.J., Bernal, B., Nahlik, A.M., Mander, Ü., Zhang, L., Anderson, C.J., Jørgensen, S.E., Brix, H., 2013. Wetlands, carbon, and climate change. Landscape Ecology 28, 583–597. https://doi.org/10.1007/s10980-012-9758-8.

Moffett, J.W., Zika, R.G., 1987. Reaction kinetics of hydrogen peroxide with copper and iron in seawater. Environmental Science & Technology 21, 804–810. https://doi.org/10.1021/es00162a012.

Moorhead, D.L., Sinsabaugh, R.L., 2000. Simulated patterns of litter decay predict patterns of extracellular enzyme activities. Applied Soil Ecology 14, 71–79. https://doi.org/10.1016/S0929-1393(99)00043-8.

Mote, P.W., Li, S., Lettenmaier, D.P., Xiao, M., Engel, R., 2018. Dramatic declines in snowpack in the western US. Npj Climate and Atmospheric Science 1, 1–6. https://doi.org/10.1038/s41612-018-0012-1.

Muñoz, C., Guillén, F., Martínez, A.T., Martínez, M.J., 1997. Laccase isoenzymes of Pleurotus eryngii: characterization, catalytic properties, and participation in activation of molecular oxygen and Mn2+ oxidation. Applied and Environmental Microbiology 63, 2166–2174.

Naughton, H.R., Keiluweit, M., Tfaily, M.M., Dynes, J.J., Regier, T., Fendorf, S., 2021. Development of energetic and enzymatic limitations on microbial carbon cycling in soils. Biogeochemistry 153, 191–213. https://doi.org/10.1007/s10533-021-00781-z.

Nguyen, N.H., Song, Z., Bates, S.T., Branco, S., Tedersoo, L., Menke, J., Schilling, J.S., Kennedy, P.G., 2016. FUNGuild: an open annotation tool for parsing fungal community datasets by ecological guild. Fungal Ecology 20, 241–248. https://doi.org/10.1016/j.funeco.2015.06.006.

Nilsson, R.H., Larsson, K.-H., Taylor, A.F.S., Bengtsson-Palme, J., Jeppesen, T.S., Schigel, D., Kennedy, P., Picard, K., Glöckner, F.O., Tedersoo, L., Saar, I., Kõljalg, U., Abarenkov, K., 2019. The UNITE database for molecular identification of fungi: handling dark taxa and parallel taxonomic classifications. Nucleic Acids Research 47, D259–D264. https://doi.org/10.1093/nar/gky1022.

Oldham, V.E., Mucci, A., Tebo, B.M., Luther, G.W., 2017. Soluble Mn(III)–L complexes are abundant in oxygenated waters and stabilized by humic ligands. Geochimica et Cosmochimica Acta 199, 238–246. https://doi.org/10.1016/j.gca.2016.11.043.

Oldham, V.E., Owings, S.M., Jones, M.R., Tebo, B.M., Luther, G.W., 2015. Evidence for the presence of strong Mn(III)-binding ligands in the water column of the Chesapeake Bay. Marine Chemistry 171, 58–66. https://doi.org/10.1016/j.marchem.2015.02.008.

Page, S.E., Kling, G.W., Sander, M., Harrold, K.H., Logan, J.R., McNeill, K., Cory, R.M., 2013. Dark Formation of hydroxyl radical in arctic soil and surface waters. Environmental Science & Technology 47, 12860–12867. https://doi.org/10.1021/es4033265.

Page, S.E., Rieley, J.O., Banks, C.J., 2011. Global and regional importance of the tropical peatland carbon pool. Global Change Biology 17, 798–818. https://doi.org/10.1111/j.1365-2486.2010.02279.x.

Perez, J., Jeffries, T.W., 1992. Roles of manganese and organic acid chelators in regulating lignin degradation and biosynthesis of peroxidases by Phanerochaete chrysosporium. Applied and Environmental Microbiology 58, 2402–2409.

Pignatello, J.J., Oliveros, E., MacKay, A., 2006. Advanced oxidation processes for organic contaminant destruction based on the Fenton reaction and related chemistry. Critical

Reviews in Environmental Science and Technology 36, 1–84. https://doi.org/10.1080/10643380500326564.

Popp, J.L., Kalyanaraman, B., Kirk, T.K., 1990. Lignin peroxidase oxidation of manganese (2+) in the presence of veratryl alcohol, malonic or oxalic acid, and oxygen. Biochemistry 29, 10475–10480. https://doi.org/10.1021/bi00498a008.

Poulton, S.W., Canfield, D.E., 2005. Development of a sequential extraction procedure for iron: implications for iron partitioning in continentally derived particulates. Chemical Geology 214, 209–221. https://doi.org/10.1016/j.chemgeo.2004.09.003.

Saiya-Cork, K.R., Sinsabaugh, R.L., Zak, D.R., 2002. The effects of long term nitrogen deposition on extracellular enzyme activity in an *Acer saccharum* forest soil. Soil Biology and Biochemistry 34, 1309–1315. https://doi.org/10.1016/S0038-0717(02)00074-3.

Schimel, J.P., Weintraub, M.N., 2003. The implications of exoenzyme activity on microbial carbon and nitrogen limitation in soil: a theoretical model. Soil Biology and Biochemistry 35, 549–563. https://doi.org/10.1016/S0038-0717(03)00015-4.

Schloss, P.D., Westcott, S.L., Ryabin, T., Hall, J.R., Hartmann, M., Hollister, E.B., Lesniewski, R.A., Oakley, B.B., Parks, D.H., Robinson, C.J., Sahl, J.W., Stres, B., Thallinger, G.G., Horn, D.J.V., Weber, C.F., 2009. Introducing mothur: open-source, platform-independent, community-supported software for describing and comparing microbial communities. Applied and Environmental Microbiology 75, 7537–7541. https://doi.org/10.1128/AEM.01541-09.

Shah, F., Schwenk, D., Nicolás, C., Persson, P., Hoffmeister, D., Tunlid, A., 2015. Involutin is an Fe3+ reductant secreted by the ectomycorrhizal fungus *Paxillus involutus* during fenton-based decomposition of organic matter. Applied and Environmental Microbiology 81, 8427–8433. https://doi.org/10.1128/AEM.02312-15.

Sheng, Y., Abreu, I.A., Cabelli, D.E., Maroney, M.J., Miller, A.-F., Teixeira, M., Valentine, J.S., 2014. Superoxide dismutases and superoxide reductases. Chemical Reviews 114, 3854–3918. https://doi.org/10.1021/cr4005296.

Sinsabaugh, R.L., 2010. Phenol oxidase, peroxidase and organic matter dynamics of soil. Soil Biology and Biochemistry 42, 391–404. https://doi.org/10.1016/j.soilbio.2009.10.014.

Sinsabaugh, R.L., Antibus, R.K., Linkins, A.E., McClaugherty, C.A., Rayburn, L., Repert, D., Weiland, T., 1992. Wood decomposition over a first-order watershed: mass loss as a function of lignocellulase activity. Soil Biology and Biochemistry 24, 743–749. https://doi.org/10.1016/0038-0717(92)90248-V.

Sinsabaugh, R.L., Moorhead, D.L., 1994. Resource allocation to extracellular enzyme production: a model for nitrogen and phosphorus control of litter decomposition. Soil Biology and Biochemistry 26, 1305–1311. https://doi.org/10.1016/0038-0717(94)90211-9.

Sokol, N.W., Sanderman, J., Bradford, M.A., 2019. Pathways of mineral-associated soil organic matter formation: Integrating the role of plant carbon source, chemistry, and point of entry. Global Change Biology 25, 12–24. https://doi.org/10.1111/gcb.14482.

Srebotnik, E., Messner, K., Foisner, R., 1988. Penetrability of white rot-degraded pine wood by the lignin peroxidase of Phanerochaete chrysosporium. Applied and Environmental Microbiology 54, 2608–2614.

Talbot, J.M., Bruns, T.D., Smith, D.P., Branco, S., Glassman, S.I., Erlandson, S., Vilgalys, R., Peay, K.G., 2013. Independent roles of ectomycorrhizal and saprotrophic communities in soil organic matter decomposition. Soil Biology and Biochemistry 57, 282–291. https://doi.org/10.1016/j.soilbio.2012.10.004.

Talbot, J.M., Martin, F., Kohler, A., Henrissat, B., Peay, K.G., 2015. Functional guild classification predicts the enzymatic role of fungi in litter and soil biogeochemistry. Soil Biology and Biochemistry 88, 441–456. https://doi.org/10.1016/j.soilbio.2015.05.006.

Tong, M., Yuan, S., Ma, S., Jin, M., Liu, D., Cheng, D., Liu, X., Gan, Y., Wang, Y., 2016. Production of abundant hydroxyl radicals from oxygenation of subsurface sediments. Environmental Science & Technology 50, 214–221. https://doi.org/10.1021/acs.est.5b04323.

Trusiak, A., Treibergs, L., Kling, G., Cory, R., 2018. The controls of iron and oxygen on hydroxyl radical (•OH) production in soils. Soil Systems 3, 1. https://doi.org/10.3390/soilsystems3010001.

Van Bodegom, P.M., Broekman, R., Van Dijk, J., Bakker, C., Aerts, R., 2005. Ferrous iron stimulates phenol oxidase activity and organic matter decomposition in waterlogged wetlands. Biogeochemistry 76, 69–83. https://doi.org/10.1007/s10533-005-2053-x.

Vidal, A., Klöffel, T., Guigue, J., Angst, G., Steffens, M., Hoeschen, C., Mueller, C.W., 2021. Visualizing the transfer of organic matter from decaying plant residues to soil mineral surfaces controlled by microorganisms. Soil Biology and Biochemistry 160, 108347. https://doi.org/10.1016/j.soilbio.2021.108347.

Walthert, L., Graf, U., Kammer, A., Luster, J., Pezzotta, D., Zimmermann, S., Hagedorn, F., 2010. Determination of organic and inorganic carbon, δ^{13} C, and nitrogen in soils containing carbonates after acid fumigation with HCl. Journal of Plant Nutrition and Soil Science 173, 207–216. https://doi.org/10.1002/jpln.200900158.

Wang, Y., Wang, H., He, J.-S., Feng, X., 2017. Iron-mediated soil carbon response to water-table decline in an alpine wetland. Nature Communications 8, 1–9. https://doi.org/10.1038/ncomms15972.

Wolf, D.C., Skipper, H.D., 1994. Soil sterilization. In: Weaver, R.W., Angle, S., Bottomley, P., Bezdicek, D., Smith, S., Tabatabai, A., Wollum, A. (Eds.), Methods of Soil Analysis: Part 2 Microbiological and Biochemical Properties. John Wiley & Sons, Ltd, Madison, Wisconsin, pp. 41–51. https://doi.org/10.2136/sssabookser5.2.c3.

Wong, D.W.S., 2009. Structure and action mechanism of ligninolytic enzymes. Applied Biochemistry and Biotechnology 157, 174–209. https://doi.org/10.1007/s12010-008-8279-z.

Xiang, W., Wan, X., Yan, S., Wu, Y., Bao, Z., 2013. Inhibitory effects of drought induced acidification on phenol oxidase activities in Sphagnum -dominated peatland. Biogeochemistry 116, 293–301. https://doi.org/10.1007/s10533-013-9859-8.

Xie, W., Yuan, S., Tong, M., Ma, S., Liao, W., Zhang, N., Chen, C., 2020. Contaminant degradation by •OH during sediment oxygenation: dependence on Fe(II) species. Environmental Science & Technology 54, 2975–2984. https://doi.org/10.1021/acs.est.9b04870.

Yuan, X., Liu, T., Fox, P., Bhattacharyya, A., Dwivedi, D., Williams, K.H., Davis, J.A., Waite, T.D., Nico, P.S., 2022. Production of hydrogen peroxide in an intra-meander hyporheic zone at East River, Colorado. Scientific Reports 12, 712. https://doi.org/10.1038/s41598-021-04171-1.

Zibilske, L.M., Bradford, J.M., 2007. Oxygen effects on carbon, polyphenols, and nitrogen mineralization potential in soil. Soil Science Society of America Journal 71, 133–139. https://doi.org/10.2136/sssaj2006.0167.